Surface-Enhanced Raman Scattering Sensors Employing a Nanoparticle-on-Liquid-Mirror (NPoLM) Architecture

*Shreyan Datta, Shoaib Vasini, Xianglong Miao and Peter Q. Liu**

Department of Electrical Engineering, University at Buffalo, The State University of New York, Buffalo, NY 14260, USA

*pqliu@buffalo.edu

Keywords: surface-enhanced Raman scattering, sensing, liquid metal, plasmonics, nanophotonics

Abstract

Surface-enhanced Raman scattering (SERS) sensors typically employ nanophotonic structures which support high field confinement and enhancement in hotspots to increase the Raman scattering from target molecules by orders of magnitude. In general, high field and SERS enhancement can be achieved by reducing the critical dimensions and mode volumes of the hotspots to nanoscale. To this end, a multitude of SERS sensors employing photonic structures with nanometric hotspots have been demonstrated. However, delivering analyte molecules into nanometric hotspots is challenging, and the trade-off between field confinement/enhancement and analyte delivery efficiency is a critical limiting factor for the performance of many nanophotonic SERS sensors. Here, we demonstrate a new type of SERS sensor employing solid-metal (e.g., gold) nanoparticles and bulk liquid metal to form nanophotonic resonators with a nanoparticle-on-liquid-mirror (NPoLM) architecture, which effectively resolves this trade-off. In particular, this unconventional sensor architecture allows for convenient formation of nanometric hotspots by introducing liquid metal after analyte molecules have been efficiently delivered to the surface of gold nanoparticles. In addition, a cost-effective and reliable process is developed to produce gold nanoparticles on a substrate suitable for forming NPoLM structures. These NPoLM structures achieve two orders of magnitude higher SERS signals than the gold nanoparticles alone.

1. Introduction

Surface-enhanced Raman scattering (SERS) is a highly effective and sensitive technique to detect molecules in trace concentrations, and finds applications in a wide range of industries such as health care, pharmaceuticals, food safety and forensics [1-3]. SERS often employs nanostructures made of metals (such as gold, silver, aluminum) to enhance the Raman signals of analytes. Such metallic nanostructures support plasmonic resonances and host electric field hotspots, whereas the intensity of the Raman signal generated by a molecule in a hotspot scales approximately to the 4th power of the local electric field enhancement factor [4]. In general, smaller hotspots with tighter electric field confinement result in stronger Raman signals, which facilitate more sensitive detection and quantification of trace analytes.

A variety of metallic nanoparticles (NPs) such as nanospheres, nanorods, nanopillars and nanostars, as well as fabricated nanostructures of different shapes, sizes and configurations have been utilized for developing SERS sensors [5-17]. Furthermore, forming dimers, oligomers or composite structures of metallic NPs can lead to nanometric gaps between the NPs, which function as hotspots with exceedingly high field enhancement and hence much larger SERS enhancement [3,18-20]. However, delivering the analyte into such nanometric hotspots can be a considerably challenging task, as the trace amount of target analyte molecules dispersed in a liquid or gas medium diffuse into the hotspots by chance, the probability of which drastically decreases as the critical dimensions of the hotspots become comparable to the sizes of the analyte molecules. Several techniques have been developed to concentrate analyte molecules and facilitate analyte delivery, such as micro- and nano-fluidics [21,22], selective wetting (i.e., creating superhydrophobic region around the sensing region) [23], and designing nanophotonic structures with passive analyte trapping capability [24]. However, these techniques do not fundamentally overcome the challenge of delivering molecules into nanometric hotspots. A strategy of forming nanometric hotspots after the analyte delivery was recently demonstrated by exploiting liquid-metal-based nanophotonic structures for surface-enhanced infrared absorption sensing [25]. Here, we apply this unconventional strategy to SERS sensing and demonstrate that combining cost-effective conventional SERS substrates consisting of solid-metal NPs with a bulk liquid metal in a straightforward way can lead to a new type of SERS sensor with a NP-on-liquid-mirror (NPoLM) architecture, which effectively resolves the trade-off between field confinement/enhancement and

analyte delivery efficiency, and achieve substantial improvement of SERS performance by two orders of magnitude.

2. Results and Discussion

2.1. NPoLM SERS Sensor Design and Operation Principle

The schematic representations of a conventional SERS substrate and our NPoLM SERS sensors are shown in Figure 1a-b. The conventional SERS substrate illustrated in Figure 1a consists of hemispherical metallic NPs (e.g., Au-NPs) on a substrate. When the distances between neighboring NPs are sufficiently large so that they do not form NP dimers or oligomers, the hotspots associated with individual NPs are not highly confined to the nanometric scale, as shown by the simulated near-field profiles in Figure 1c. In this configuration, analyte molecules in a liquid or gas medium can be delivered to the NP surface (including the hotspot regions) with relatively high efficiency, as the molecules simply get adsorbed on the well-exposed NP surface which does not feature nanometric gaps. However, owing to the relatively moderate field confinement/enhancement in the hotspots of individual NPs, the SERS performance of such conventional SERS substrates consisting of individual NPs without sharp tips or nanometric gaps is typically modest.

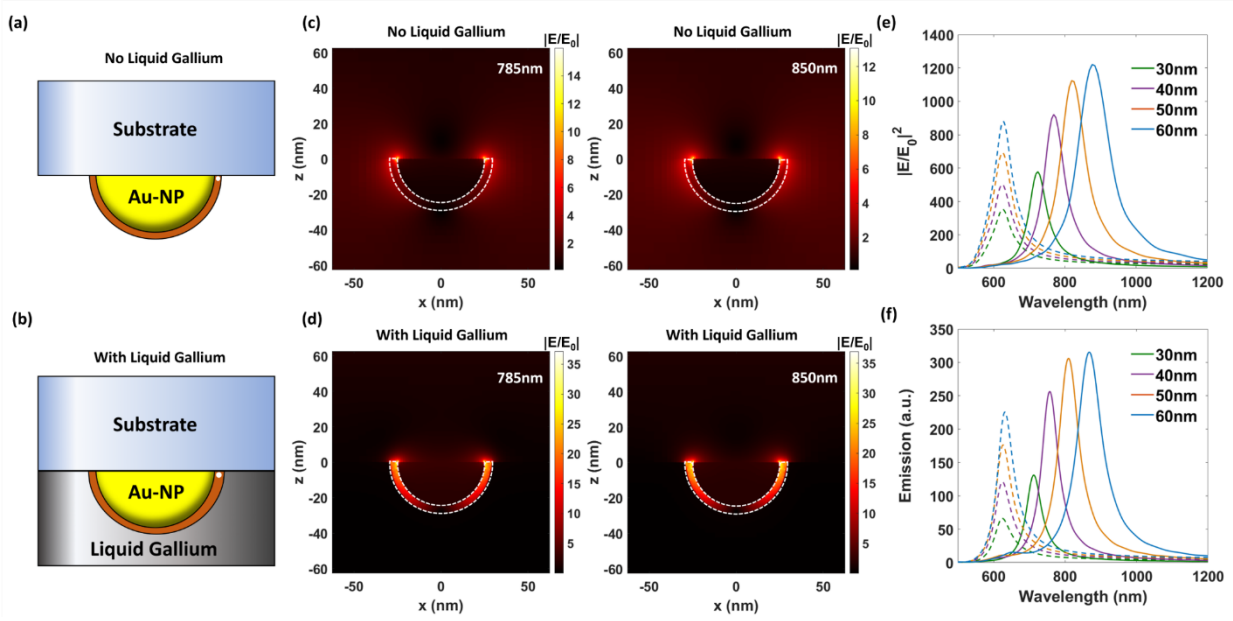

Figure 1. Comparison between individual NPs and NPoLM structures. (a) Schematic of a conventional SERS substrate with individual Au-NPs. (b) Schematic of the proposed NPoLM SERS sensor. The orange

arc in the schematics in (a) and (b) represents analyte molecules adsorbed on the Au-NP surface. (c) Simulated electric field enhancement ($|E/E_0|$) profiles of an individual Au-NP (50 nm NP diameter) at 785 nm and 850 nm wavelengths. (d) Simulated electric field enhancement ($|E/E_0|$) profiles of a NPoLM structure (50 nm NP diameter) at 785 nm and 850 nm wavelengths. (e) Simulated electric field intensity enhancement factor (i.e., $|E/E_0|^2$) as functions of wavelength for different individual Au-NPs (dashed lines) and the corresponding NPoLM structures (solid lines) with the specified NP diameters. (f) Simulated dipole source emission spectra for different individual Au-NPs (dashed lines) and the corresponding NPoLM structures (solid lines) with the specified NP diameters. The position of the dipole source is marked by the white dot in (a) and (b).

Taking advantage of the fluidic nature and hence high conformability of a liquid metal near room temperature (e.g., liquid gallium), we can cover the analyte-coated NPs with liquid metal to form the proposed NPoLM structure illustrated in Figure 1b. Such a NPoLM structure essentially functions as a nanopatch antenna resonator with hotspots in the gap between the NP surface and the liquid metal, as shown in the near-field profiles in Figure 1d. These hotspots are fully occupied by the adsorbed analyte molecules and can reach much higher field confinement/enhancement than the NP alone, especially when the adsorbed analyte molecules on the NP surface only form a thin nanometric layer (e.g., a few molecular layers or less). In addition, the hotspots of the NPoLM structure occupies a relatively large portion of the NP surface area, which is substantially larger than that of the conventional NP-on-mirror structure consisting of a spherical NP on a flat solid metal surface [26]. The optical response of the NPoLM structure is not sensitive to the dielectric substrate as the highly confined field in the gap has insignificant overlap with the substrate.

Since the nanometric hotspots of such a NPoLM structure are formed after the efficient adsorption of analyte molecules on the well-exposed NP surface, the proposed NPoLM SERS sensor leads to both high analyte delivery efficiency and high field confinement, hence fundamentally resolves the trade-off between these two crucial factors. Furthermore, the NPoLM structure provides another two key advantages for SERS. First, compared to an individual NP whose plasmonic resonance is not sensitive to the NP size, the resonance of the NPoLM structure is strongly dependent on the NP size, as revealed by the simulated spectra in Figures 1e-f. Consequently, employing the NPoLM structure for SERS allows for matching the nanophotonic resonance to the Raman excitation laser by choosing the appropriate NP size, which in turn leads to higher SERS

enhancement. For example, as shown in Figure 1e, the hemispherical Au-NPs with different sizes all exhibit plasmonic resonances near 600 nm, and their near-field enhancement at 785 nm (a popular wavelength for Raman spectroscopy) is relatively weak. On the other hand, the resonances of the corresponding NPoLM structures span across more than 200 nm wavelength range (~700 to 900 nm) when the NP diameter varies from 30 to 60 nm (the analyte film thickness is assumed to be 4 nm). The NPoLM structure based on NP with a 40 or 50 nm diameter has its resonance near 785 nm, leading to much higher field enhancement in the hotspots than the NP alone at this popular Raman spectroscopy wavelength (see Figure 1e). Another key advantage is evident in Figure 1f, which shows that the simulated emission spectra of individual NPs and the corresponding NPoLM structures, assuming a point dipole source is placed inside their hotspots. The NPoLM structures clearly produce much stronger emission at their resonances, which is a consequence of the higher field enhancement in their hotspots. Therefore, the NPoLM structures can facilitate the emission of Raman scattered photons much more significantly across a wide wavelength range than individual NPs alone.

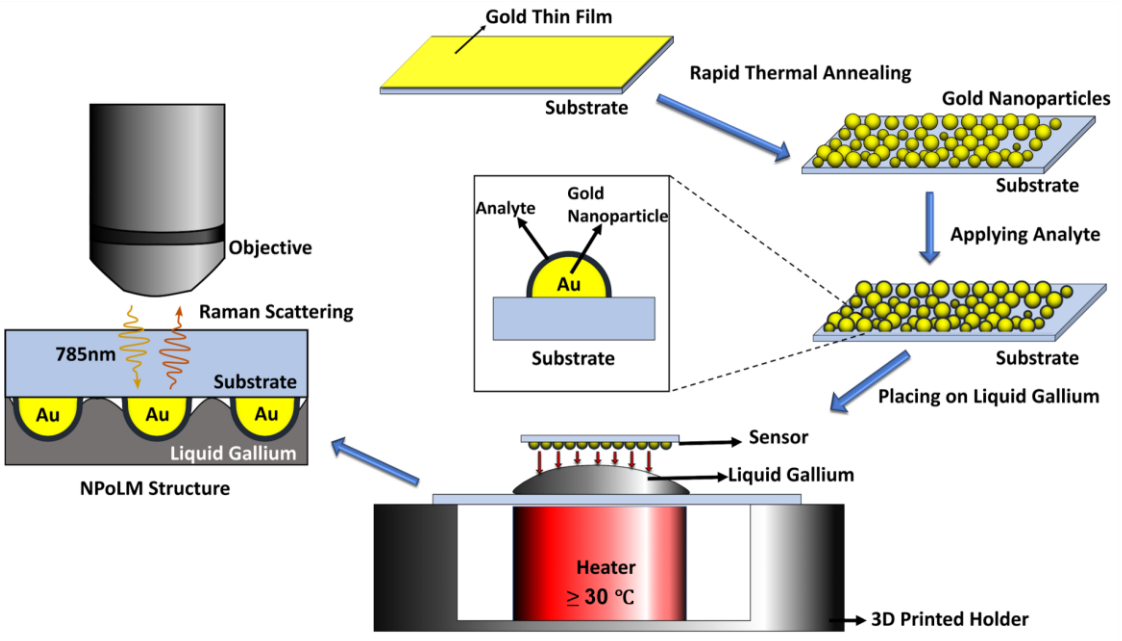

Figure 2. Schematics of the device fabrication and analyte sensing procedures for the NPoLM SERS sensor.

2.2. Device Fabrication

Figure 2 shows the schematics of the device fabrication and analyte sensing procedures for our NPoLM SERS sensor. To achieve cost-effective fabrication of the SERS substrate consisting of Au-NPs on a substrate, we developed a simple and reliable process based on rapid thermal annealing (RTA) of ultra-thin Au film deposited on sapphire substrate (see **Experimental Section**) [27]. After introducing the analyte to the SERS substrate which can be conducted using any conventional approach, the SERS substrate is then gently placed on the surface of a small amount of liquid metal to form the complete structure of the NPoLM SERS sensor. Subsequently, Raman spectra can be measured from the substrate side to obtain the Raman signals associated with the target analyte molecules. We employ liquid Ga to form the NPoLM structures because liquid Ga remains in its liquid phase near room temperature and has various appealing material properties for photonics applications [28]. Alternatively, several Ga-rich alloys that have similar mechanical and optical properties as Ga, such as eutectic Ga-In (EGaIn) and Ga-In-Sn (Galinstan), can also be used as the room-temperature liquid metal to form NPoLM structures [28]. In our experiment, a small volume (~ 50 μL) of liquid Ga is placed on a glass microscope slide which sits on a 3D-printed sample holder. To guarantee that liquid Ga does not solidify during the experiment, a small heater is installed in the sample holder just below the microscope slide to keep the liquid Ga temperature slightly above 30 °C. A plastic swab is used to scrape the surface of the liquid Ga and expose a shiny mirror-like surface, and then the SERS substrate is quickly but gently placed on the liquid Ga surface. This contact process is simple and requires no special instrument, and therefore is highly suitable for field-deployable and point-of-care applications.

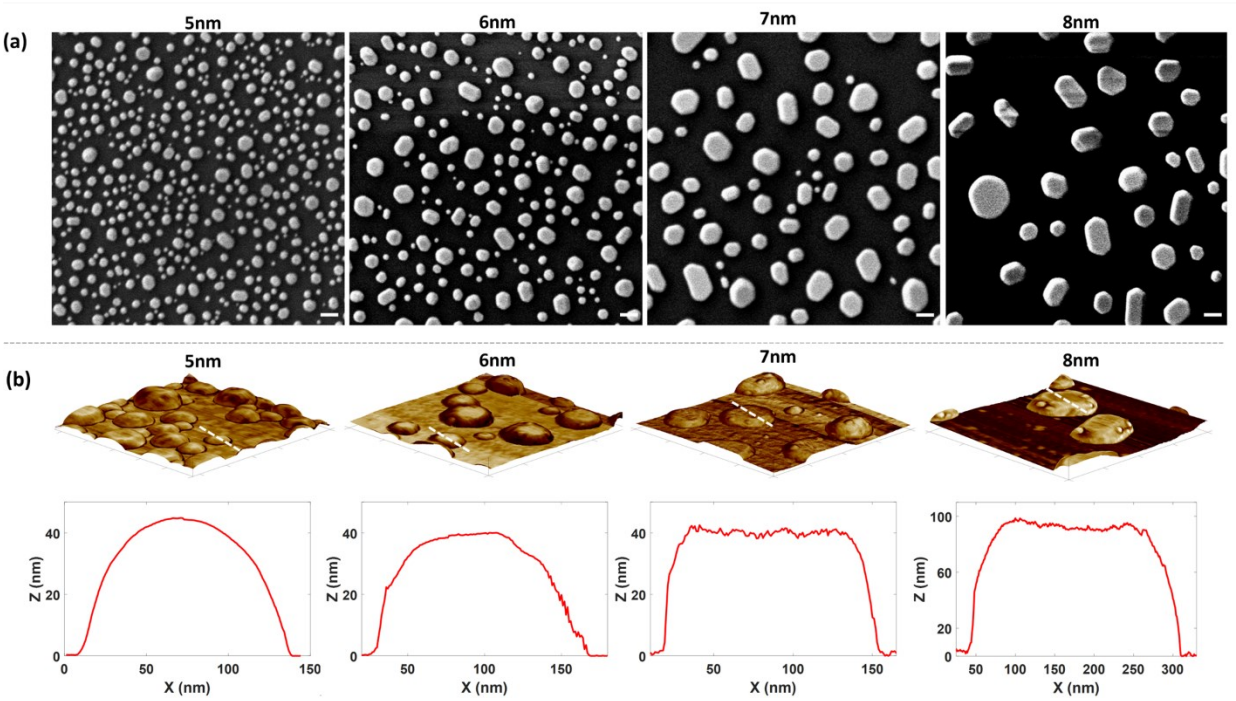

Figure 3. Characterization of RTA-produced Au-NPs. (a) SEM images of Au-NPs produced by RTA of Au thin films with different thicknesses deposited on sapphire substrate. The scale bars are 100 nm long. (b) Rendered perspective AFM images and cross-sectional line profiles of Au-NPs produced by RTA of Au thin films with different thicknesses deposited on sapphire substrate.

The size distribution of Au-NPs formed by the RTA method sensitively dependents on the thickness of the deposited Au thin film, which provides an effective way to tune the resonances of the NPoLM structures to match specific Raman excitation laser wavelength. Figure 3 shows the scanning electron microscopy (SEM) and atomic force microscopy (AFM) images of several fabricated SERS substrates with Au-NPs produced from Au thin films of different thicknesses (i.e., 5 to 8 nm). As can be clearly seen in Figure 3a, thicker Au film leads to larger RTA-produced Au-NPs. The average size, density and surface coverage of the Au-NPs for different Au film thicknesses are listed in the **Supporting Information Table S1**. The AFM images in Figure 3b show the side and cross-sectional profiles of the Au-NPs. The typical shape of the Au-NPs gradually evolves from hemisphere to flat-topped disk, as the Au thin film thickness and hence the Au-NP sizes increase. Although the Au-NPs are randomly distributed on the sapphire substrate, they do not aggregate to form dimers or oligomers. We choose sapphire as the substrate material because of the relatively strong adhesion between the Au-NPs and sapphire. We do not observe any displacement or aggregation of Au-NPs when such sapphire-based SERS substrates are immersed in a liquid analyte sample for analyte adsorption and subsequently dried. This is in sharp

contrast to the cases with glass or fused silica substrate, which has weaker adhesion with Au-NPs and may result in displacement and aggregation of Au-NPs after introducing a liquid analyte.

2.3. NPoLM SERS Sensor Performance

To benchmark the performance of the NPoLM SERS sensors, we chose 1-octadecanethiol (ODT) as the target analyte molecule. ODT is an alkanethiol which has strong affinity to Au surface due to the presence of the thiol (-SH) group. This strong affinity results in reliable formation of a self-assembled monolayer (SAM) of ODT molecules on Au surface [29]. Nevertheless, the NPoLM SERS sensors are not limited to sensing molecules with a thiol group, but can be used to sense any type of analyte molecules that can adsorb or precipitate (after drop casting and solvent evaporation) on Au surface. To form the SAM ODT layer on the surface of the Au-NPs on our SERS substrates, the substrates were immersed in an ethanol-based ODT solution for 8 to 12 hours, after which the SERS substrates were thoroughly rinsed in ethanol for more than a minute and blown dry. The rinsing ensured the removal of any excess unbonded ODT molecule from the surface of the SERS substrate (see **Experimental Section**).

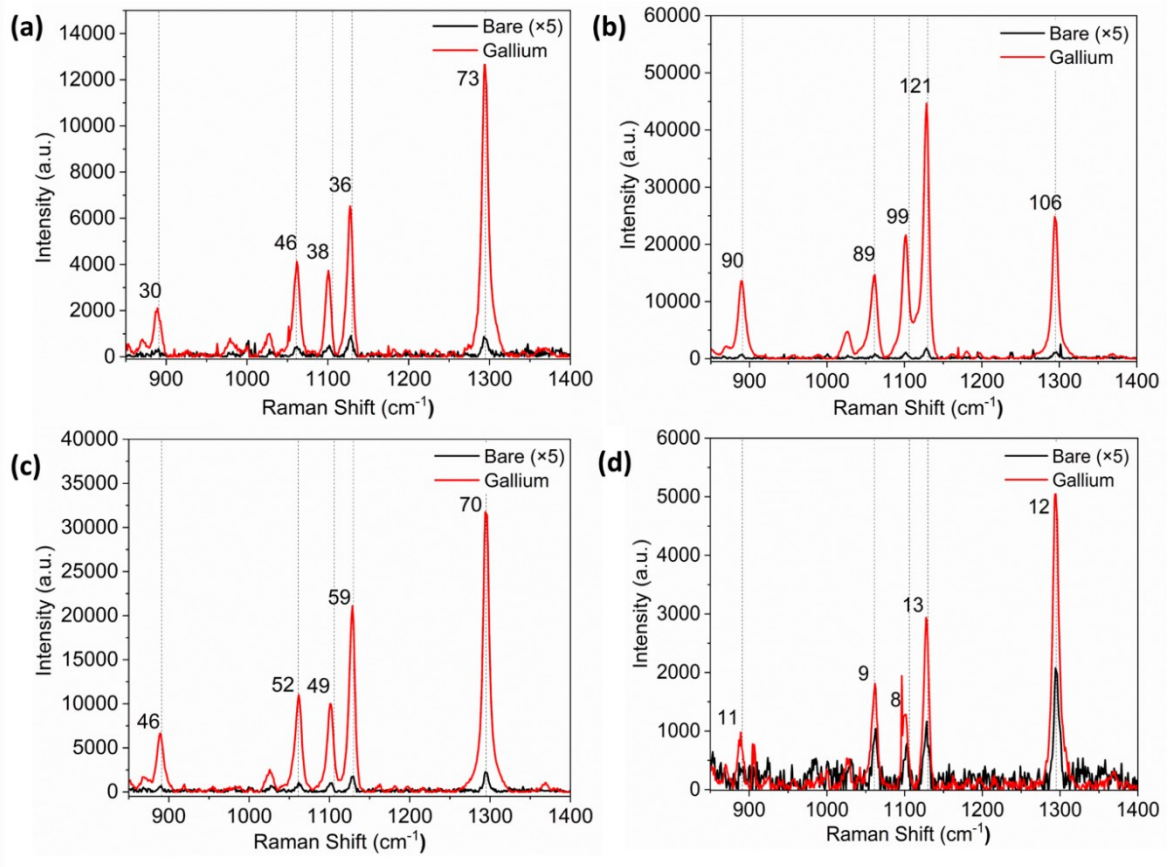

Figure 4. Comparison of the Raman spectra of SAM ODT obtained from the SERS substrates with bare Au-NPs (i.e., before introducing liquid Ga, black lines) and the corresponding NPoLM SERS sensors (i.e., after introducing liquid Ga, red lines). The 4 panels correspond to the sensors produced from (a) 5 nm, (b) 6 nm, (c) 7 nm, and (d) 8 nm thick Au thin films on sapphire substrate. Baseline subtraction has been applied to all the Raman spectra. The Raman spectra obtained from the bare Au-NPs are multiplied by a factor of 5 to enhance their visibility in the plots. The relative enhancement factors as a result of introducing liquid Ga to form the NPoLM structures are labeled next to each ODT Raman peak.

We characterized the Raman spectra of the SAM-ODT-coated sensors both before and after forming the NPoLM structures (see Experimental Section). After gently placing the Au-NP side of the sensor chip on liquid Ga to form the NPoLM structures, the chip surface usually exhibits a clean and uniform texture (see **Supporting Information Figure S1**), indicating high-quality contact between the liquid Ga and the SAM-ODT-coated Au-NPs. The excitation laser wavelength was at 785 nm and only the Stokes Raman peaks were collected. For the SERS substrates with Au-NPs alone (i.e., before introducing liquid Ga), the Raman spectra were measured from both the Au-NP side and the sapphire substrate side, and we observed that the Raman signals measured from the substrate side were significantly higher than those measured from the NP side. This is consistent with the fact that a dipole source near a dielectric/air interface emits more light into the dielectric than air. Therefore, we always compare the higher Raman signals measured from the substrate side of a SERS substrate to the Raman signals from the corresponding NPoLM structrure (i.e., after introducing liquid Ga). Figure 4 shows the comparison between the Raman spectra measured before and after introducing liquid Ga to form the NPoLM structures for four different SAM-ODT-coated sensors (corresponding to the specified four different thicknesses of the annealed Au thin films). Each Raman spectrum plotted in Figure 4 is the average of the measurements at multiple (10 or more) randomly selected locations on the sensor surface and therefore represents the typical SERS performance of the sensor. Multiple Raman peaks of the ODT molecules can be observed in these spectra, with the strongest peaks located at around 891 cm^{-1}, 1061 cm^{-1}, 1106 cm^{-1}, 1130 cm^{-1}, and 1295 cm^{-1}, respectively. Evidently, all the NPoLM structures produced much higher ODT Raman signals than the Au-NPs alone. The relative enhancement factor (i.e., the ratio of the Raman peak intensity obtained from the NPoLM structures to that from the corresponding Au-NPs alone) for each dominant ODT Raman peak is

labeled next to the Raman peaks in Figure 4. The NPoLM SERS sensor based on Au-NPs produced from 6 nm Au thin film exhibits the highest relative enhancement factors for the 5 dominant ODT Raman peaks, which are approximately two orders of magnitude (ranging from 90 to 120, see Figure 4b). The relative enhancement factors associated with the sensors produced from 5 nm (Figure 4a) and 7 nm (Figure 4c) Au thin films range from 30 to 70, whereas they reduce to around 10 for the sensor produced from 8 nm Au thin film (Figure 4d). For SERS sensing of ODT with a 785 nm excitation laser, the wavelengths of the ODT Raman signals are around 850 nm, and therefore the optimal nanophotonic resonance should be close to 820 nm for achieving high SERS enhancement [30]. If we use the average Au-NP diameter of the best-performing NPoLM sensor (i.e., 60 nm) in the simulation model, the effective gap size is found to be approximately 5 nm to result in a NPoLM resonance near 820 nm (see **Supporting Information Figure S2**). This is in good agreement with our expectation, because in addition to the SAM ODT (~2.5 nm thick), the nanometric native oxide layer on the liquid Ga surface and the surface roughness of the Au-NPs contribute to the effective gap size in the few nm range [25]. Larger or smaller NPs result in longer or shorter NPoLM resonant wavelengths compared to the optimal value, and hence a reduction in the SERS enhancement factor. We also characterized the absolute ensemble-level SERS enhancement factors of our sensors (see **Supporting Information**), which fall in the range of 10^4 to 4×10^4 for the Au-NPs alone, and in the range of 9×10^5 to 4×10^6 for the NPoLM structures based on the Au-NPs produced from 6 nm Au thin film (in Figure 4b). Note that the contact between the ODT molecules with -CH_3 termination and the liquid Ga with a native oxide layer is not expected to alter the state of the ODT molecules, as this contact interface is a van der Waals interface with weak contact interactions [31]. Another appealing attribute of the demonstrated NPoLM SERS sensor is that its intra-sample SERS signal variation is generally smaller than that of the Au-NPs alone (see **Supporting Information Table S2**). In addition, after the Raman measurement, the liquid Ga can be completely removed from the chip surface and no change to the ODT-coated Au-NPs were observed (see **Supporting Information Figure S3**).

To gain further insights into the dependence of the NPoLM SERS sensor performance on the NP size distribution, we fabricated uniform arrays of Au nanodisks (Au-NDs) with precisely defined diameters using electron beam lithography and template stripping (see **Experimental Section**), and employed these Au-ND arrays to conduct the same SERS sensing experiments as we did with the RTA-produced Au-NPs. The template stripping method has been frequently used to fabricate

metallic nanostructures with relatively small surface roughness [32,33]. The diameters of the Au-NDs range from 60 to 90 nm (see Figure 5a), which are comparable to the typical values of the RTA-produced Au-NPs. Figure 5b shows the reflection spectra of the different Au-ND arrays and the corresponding ND-on-liquid-mirror (NDoLM) structures with a SAM ODT on the Au-ND surface. Since each array contains Au-NDs of the same size, the reflection spectrum of the array exhibits a single prominent resonance, which is also an indication of the successful formation of the complete NDoLM structures. As expected, the localized plasmonic resonance of each bare Au-ND array shows weak dependence on the ND diameter and is far from 785 nm, whereas the NDoLM resonance is widely tunable by changing the Au-ND diameter. In particular, the NDoLM array based on 60 nm Au-ND has its resonance near 800 nm, which should be the optimal one among the different arrays for SERS with 785 nm excitation wavelength. Indeed, as shown in Figure 5c, the 60 nm NDoLM structure produced the strongest SERS signals for all five dominant ODT Raman peaks. As the Au-ND diameter increasingly deviates from the optimal value, the NDoLM resonance shifts further away from 800 nm, and consequently the SERS signals significantly reduce. This is also a strong evidence that the observed SERS enhancement is a resonant electromagnetic effect rather than a chemical effect [34]. Furthermore, these experimental observations indicate that the liquid Ga surface itself does not produce any significant SERS enhancement when an IR excitation laser (e.g., 785 nm) is used.

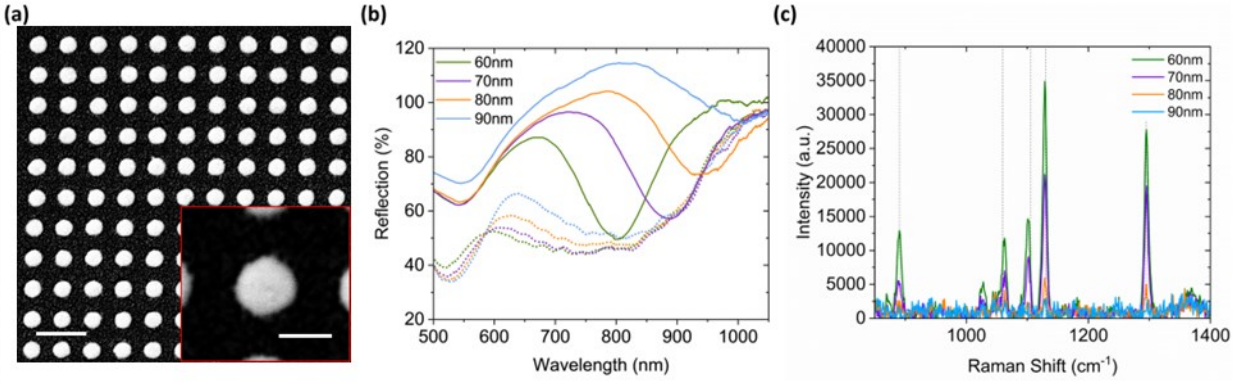

Figure 5. Experimental results from the EBL-fabricated Au-NDs and corresponding NDoLM structures. (a) SEM image of an EBL-fabricated Au-ND array with 60 nm ND diameter. The inset shows a zoomed-in view of a single Au-ND. The scale bar is 200 nm long in the main image, and 60 nm long in the inset image. (b) Reflection spectra of different Au-ND arrays (dashed lines) and the corresponding NDoLM arrays (solid lines) for different ND diameters. (c) Comparison of the Raman spectra of SAM ODT obtained from the NDoLM structures with different Au-ND diameters. Baseline subtraction was applied to all Raman spectra.

3. Conclusion

In summary, we experimentally demonstrate that employing liquid metal and conventional SERS substrates to form NPoLM structures using a simple process can lead to substantial improvement in SERS performance by two orders of magnitude. A low-cost lithography-free process based on RTA of Au thin film is developed to fabricate the conventional SERS substrates consisting of non-clustered Au-NPs, with the size distribution of the Au-NPs sensitively dependent on the Au thin film thickness. As the nanometric hotspots of the NPoLM structures are formed by introducing the liquid metal after the efficient delivery of analyte molecules to the conventional SERS substrates without preformed nanometric hotspots, the NPoLM device architecture represents an effective strategy to overcome the trade-off between field confinement and analyte delivery efficiency. Furthermore, the resonances of the NPoLM structures can be widely tuned to match the Raman excitation laser wavelength by controlling the NP size, which is another key advantage over the conventional SERS substrates consisting of individual NPs with plasmonic resonances of limited tunability. This proof-of-concept demonstration may lead to further development of various forms of liquid-metal-based nanophotonic SERS sensors for a wide range of molecular species and chemical-/bio-sensing applications.

4. Experimental Section

Fabrication of Au-NP-based SERS substrates using RTA

Double-side polished 165 μm thick sapphire substrates were first cleaned by ultrasonication in acetone and isopropyl alcohol, followed by an oxygen plasma treatment at 300 mT pressure for 120 seconds. Thin Au films with thicknesses ranging from 5 nm to 8 nm were deposited on the cleaned sapphire substrates using a Kurt J. Lesker AXXIS electron-beam evaporator. The samples were then annealed in an Ulvac Technology MILA 3000 RTA tool at 800°C for 30 seconds to transform the Au thin films on the sapphire substrates into Au-NPs with different size distributions. A ramp duration of 40 seconds was used to reach 800°C.

Fabrication of Au-ND-based SERS substrates using electron beam lithography and template stripping

A 100 kV electron-beam lithography system (Elionix ELS-G100) was used to pattern arrays of nano-holes with various diameters in a PMMA double-layer spin-coated on a silicon substrate. A PMMA double-layer (a PMMA 495 layer followed by a PMMA 950 layer) was used to facilitate the lift-off process after the Au thin film deposition. A 25 nm thick Au film was deposited on the patterned sample using the electron-beam evaporator. The sample was then immersed in acetone for lift-off, followed by rinsing in isopropyl alcohol and blown dry, which resulted in arrays of Au-NDs on the silicon substrate. Subsequently, to transfer the Au-ND arrays to a sapphire substrate with a template stripping process, the sample was first placed in a vacuum chamber next to 2 mL of 1H,1H,2H,2H-perfluorooctyl trichlorosilane (FOTS) for about 10 minutes, so that FOTS molecules could adsorb on the Si surface to weaken the adhesion between the epoxy used in the next step and the Si surface. The Au-ND arrays on the silicon substrate were then bonded to a sapphire substrate by a thin layer of epoxy (EPO-TEK 353ND). After the epoxy was fully cured, the sapphire substrate was lifted up manually, which caused the separation of the epoxy layer and the embedded Au-ND arrays from the silicon substrate surface.

Procedure to form SAM ODT on the surface of Au-NPs

An ODT solution at 1 mM concentration was prepared by dissolving 28.6 mg of solid ODT powder in 100 mL ethanol. The SERS substrates were placed in small vials containing a few mL ODT solution for 8 to 12 hours to form the SAM ODT on the surface of Au-NPs (or Au-NDs). The ODT-coated SERS substrates were then rinsed thoroughly in ethanol and blown dry to remove any excess unbonded ODT molecules.

Spectroscopy characterizations

The Raman spectra of the samples were measured using a Renishaw InVia Raman microscope system. The wavelength of the excitation laser is 785 nm, and the laser power used was 4.3 mW. A 1200 lines/mm grating in the spectrometer was selected. A 50X microscope objective with 0.75 numerical aperture (NA) was used to measure all the reported Raman spectra. The integration time was 300 s for measuring the bare Au-NPs, and 50 s for measuring the NPoLM structures.

The reflection spectra of the Au-ND array-based samples were measured with a home-build microscope setup connected to an Ocean Optics USB 2000 spectrograph via a multi-mode optical fiber. The broadband light from a stabilized tungsten-halogen light source (Thorlabs SLS201L) was focused on the samples by a 40X 0.65 NA objective, and the reflected light was collected by the same objective.

Acknowledgements

This work is supported in part by the National Science Foundation (NSF) under Award No. ECCS-1847203 and the National Cancer Institute (NCI) of the National Institutes of Health (NIH) under Award No. R01CA272827. The authors thank Dr. Yuan Li for the helpful discussions on the template stripping process.

Conflict of Interest

The authors declare no conflict of interest.

References

[1] D. L. Jeanmaire, R. P. Van Duyne, *Chem. Interfacial Electrochem.* **1977**, *84*, 1−20.

[2] M. G. Albrecht, J. A. Creighton, *J. Am. Chem. Soc.* **1977**, *99*, 5215−5217.

[3] J. Langer, D. Jimenez de Aberasturi, J. Aizpurua, R. A. Alvarez-Puebla, B. Auguie, J. J. Baumberg, G. C. Bazan, S. E. J. Bell, A. Boisen, A. G. Brolo, J. Choo, D. Cialla-May, V. Deckert, L. Fabris, K. Faulds, F. J. Garcia de Abajo, R. Goodacre, D. Graham, A. J. Haes, C. L. Haynes, et al., *ACS Nano* **2020**, *14*, 28−117.

[4] G. C. Schatz, *Acc. Chem. Res.* **1984**, *17*, 370−376.

[5] X. Qian, X.-H. Peng, D. O. Ansari, Q. Yin-Goen, G. Z. Chen, D. M. Shin, L. Yang, A. N. Young, M. D. Wang, S. Nie, *Nat. Biotechnol.* **2008**, *26*, 83−90.

[6] J. F. Li, Y. F. Huang, Y. Ding, Z. L. Yang, S. B. Li, X. S. Zhou, F. R. Fan, W. Zhang, Z. Y. Zhou, D. Y. Wu, B. Ren, Z. L. Wang, Z. Q. Tian, *Nature* **2010**, *464*, 392−395.

[7] K.-Q. Lin, J. Yi, S. Hu, B.-J. Liu, J.-Y. Liu, X. Wang, B. Ren, *J. Phys. Chem. C* **2016**, *120*, 20806-20813.

[8] M. S. Schmidt, J. Hübner, A. Boisen, *Adv. Mater.* **2012**, *24*, OP11−OP18.

[9] C. G. Khoury, T. Vo-Dinh, *J. Phys. Chem. C* **2008**, *112*, 18849−18859.

[10] L. Rodríguez-Lorenzo, R. A. Álvarez-Puebla, I. Pastoriza-Santos, S. Mazzucco, O. Stéphan, M. Kociak, L. M. Liz-Marzán, F. J. García de Abajo, *J. Am. Chem. Soc.* **2009**, *131*, 4616−4618.

[11] A. S. D. S. Indrasekara, S. Meyers, S. Shubeita, L. C. Feldman, T. Gustafsson, L. Fabris, Gold Nanostar Substrates for SERS Sensing in the Femtomolar Regime. *Nanoscale* **2014**, *6*, 8891−8899.

[12] C. L. Haynes, R. P. Van Duyne, *J. Phys. Chem. B* **2003**, *107*, 7426-7433.

[13] H. Im, K. C. Bantz, N. C. Lindquist, C. L. Haynes, S.-H. Oh, *Nano Lett.* **2010**, *10*, 2231-2236.

[14] M. Nie, Y. Zhao, W. Nam, J. Song, W. Zhu, H. J. Lezec, A. Agrawal, W. Zhou, *Adv. Funct. Mater.* **2022**, *32*, 2202231.

[15] S. Yan, J. Sun, B. Chen, L. Wang, S. Bian, M. Sawan, H. Tang, L. Wen, G. Meng, *ACS Nano* **2023**, *17*, 22766-22777.

[16] D. R. Ward, N. K. Grady, C. S. Levin, N. J. Halas, Y. Wu, P. Nordlander, D. Natelson, *Nano Lett.* **2007**, *7*, 1396−1400.

[17] L. Tian, M. Su, F. Yu, Y. Xu, X. Li, L. Li, H. Liu, W. Tan, *Nat. Commun.* **2018**, *9*, 3642.

[18] P. H. C. Camargo, L. Au, M. Rycenga, W. Li, Y. Xia, *Chem. Phys. Lett.* **2010**, *484*, 304-308.

[19] E. A. Sprague-Klein, B. Negru, L. R. Madison, S. C. Coste, B. K. Rugg, A. M. Felts, M. O. McAnally, M. Banik, V. A. Apkarian, M. R. Wasielewski, M. A. Ratner, T. Seideman, G. C. Schatz, R. P. Van Duyne, *J. Am. Chem. Soc.* **2018**, *140*, 10583−10592.

[20] R. A. Alvarez-Puebla, A. Agarwal, P. Manna, B. P. Khanal, P. Aldeanueva-Potel, E. Carbo-Argibay, N. Pazos-Perez, L. Vigderman, E. R. Zubarev, N. A. Kotov, L. M. Liz-Marzan, *Proc. Natl. Acad. Sci. U.S.A.* **2011***, 108,* 8157−8161.

[21] X. Fan, I. M. White, *Nat. Photonics* **2011**, *5*, 591–597.

[22] M. Wang, N. Jing, I. H. Chou, G. L. Cote, J. Kameoka, *Lab Chip* **2007**, *7*, 630–632.

[23] F. De Angelis, F. Gentile, F. Mecarini, G. Das, M. Moretti, P. Candeloro, M. L. Coluccio, G. Cojoc, A. Accardo, C. Liberale, R. P. Zaccaria, G. Perozziello, L. Tirinato, A. Toma, G. Cuda, R. Cingolani, E. Di Fabrizio, *Nat. Photonics* **2011**, *5*, 683−688.

[24] X. Miao, L. Yan, Y. Wu, P. Q. Liu, *Light: Sci. Appl.* **2021**, *10*, 5.

[25] X. Miao, T. S. Luk, P. Q. Liu, *Adv. Mater.* **2022**, *34*, 2107950.

[26] F. Benz, C. Tserkezis, L. O. Herrmann, B. de Nijs, A. Sanders, D. O. Sigle, L. Pukenas, S. D. Evans, J. Aizpurua, J. J. Baumberg, *Nano Lett.* **2015**, *15*, 669−674.

[27] H. T.-H. Lin, C.-K. Yang, C.-C. Lin, A. M.-H. Wu, L. A. Wang, N.-T. Huang, *Nanomaterials* **2017**, *7*, 100.

[28] P. Q. Liu, X. Miao, S. Datta, *Opt. Mater. Express* **2023**, *13*, 699-727.

[29] J. C. Love, L. A. Estroff, J. K. Kriebel, R. G. Nuzzo, G. M. Whitesides, *Chem. Rev.* **2005**, *105*, 1103-1169.

[30] R. A. Alvarez-Puebla, *J. Phys. Chem. Lett.* **2012**, *3*, 857-866.

[31] C. M. Bowers, K.-C. Liao, H. J. Yoon, D. Rappoport, M. Baghbanzadeh, F. C. Simeone, G. M. Whitesides, *Nano Lett.* **2014**, *14*, 3521-3526.

[32] N. Vogel, M. Jung, N. L. Bocchio, M. Retsch, M. Kreiter, I. Koeper, *Small* **2010**, *6*, 104-109.

[33] D. Yoo, T. W. Johnson, S. Cherukulappurath, D. J. Norris, S.-H. Oh, *ACS Nano* **2015**, *9*, 10647-10654.

[34] N. Valley, N. Greeneltch, R. P. Van Duyne, G. C. Schatz, *J. Phys. Chem. Lett.* **2013**, *4*, 2599−2604.

TOC graphic

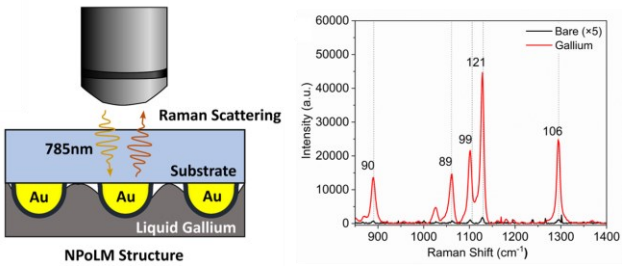

High-performance SERS sensors can be straightforwardly realized by combining a liquid metal and conventional SERS substrates consisting of solid metal nanoparticles to form nanophotonic resonators with a nanoparticle-on-liquid-mirror (NPoLM) architecture. Such NPoLM SERS sensors effectively resolve the trade-off between field confinement/enhancement and analyte delivery efficiency, leading to orders of magnitude SERS performance improvement.